Orientational ordering in films of molecular hydrogen on boron nitride: Thick (12-layer) films and bilayer films

Kiho Kim* and N. S. Sullivan
Department of Physics, University of Florida, Gainesville, Florida 32611-8440
(Received 14 June 1996; revised manuscript received 15 December 1997)

We report NMR studies of the orientational ordering of molecular hydrogen in films physisorbed on hexagonal boron nitride (BN). The local orientational ordering of the molecular axes is determined for both thick films (12 layers) and thin films (bilayers). The ordering observed is in *both* cases very different from that observed for bulk solid hydrogen. Quadrupolar glass ordering occurs for intermediate layers in thick films at low ortho concentrations $0.25<X<0.40$ and $T\leqslant 0.7$ K. The ortho molecules remain rotationally disordered in the outer layers of the thick films and invariant to small changes in thickness. In the bilayers one observes a long range ordering for $T\leqslant 1.95$ K and $X\leqslant 0.56$, and a quadrupolar glass ordering for intermediate concentrations ($0.37<X<0.55$) and intermediate temperatures ($0.7<T<1.1$ K). [S0163-1829(98)09019-5]

I. INTRODUCTION

This paper reports systematic studies of the orientational ordering in films of solid hydrogen adsorbed on hexagonal boron nitride (BN) using high-sensitivity continuous wave (CW) nuclear magnetic resonance (NMR) techniques.[1] The interest in these experiments is to determine the nature of the orientational ordering of quantum rotors in restricted geometries where as a result of the constraints and the geometrical frustration of the interactions,[2–5] new behaviors very different from those of bulk H_2 are expected for the ordering of the rotational degrees of freedom. In particular we wanted to compare the orientational ordering in thick films (12 layers) with that observed in thin films (bilayers). The surface interactions tend to align the molecular axes either parallel or perpendicular to the substrate, but this trend will compete strongly with the electrostatic quadrupole-quadrupole (EQQ) intermolecular interactions for which the molecules prefer to be mutually perpendicular. Furthermore, the enhanced quantum zero point motion (ZPM) at the free (solid/vapor) surface of the films will tend to inhibit orientational ordering near the free surface. As a result of these competing trends, periodic orientational ordering is expected to be very fragile in H_2 films, and the effects of frustration are expected to lead to very different orientational configurations for thick films compared to thin films. In addition, new orientational glasses or mixed orientational phases are expected for the constrained films for dilute ortho concentrations. In order to better understand the effects of substrate potentials and ZPM on the orientational ordering, we have studied the behavior of films of H_2 for which a systematic study could be carried out for a wide range of film thicknesses, allowing one to compare the ordering for substrate bound monolayers, very thin films (2 layers), thin films (4 and 8 layers),[6] and thick films (12 layers).

In bulk H_2 samples, it has been well established that the EQQ interactions, V_{QQ}, play the major role among the anisotropic intermolecular interactions[7–9] in determining the orientational ordering of the molecular axes at low temperatures. The molecular centers of mass remain fixed and it is the anisotropic interactions that determine the orientational ordering. It is important to note that there is a strong decoupling of the translational and rotational degrees of freedom in the solid hydrogens and the interpretation of the orientational ordering from NMR data is very robust with respect to changes or uncertainties in the translational symmetry of the lattice structures. The NMR line shapes are to a very large extent determined by the orientational ordering, and the width of the line shapes in the ordered states (~ 400 kHz) is much larger than those for orientational disorder (~ 50 kHz).

At sufficiently high temperatures, $k_BT>|V_{QQ}|$, the molecules are free to rotate and the mean orientation of each molecule is zero. At low temperatures, $k_BT<|V_{QQ}|$, the molecules adopt orientations to minimize their interaction energy, leading to orientationally ordered structures. The interactions are highly frustrated because of the incompatibility between the symmetry of the quadrupole-quadrupole interaction and the lattice geometry. In order to probe the geometrical nature of the frustration in this class of systems, a number of studies of solid hydrogen in restricted geometries (adsorbed films[10–16] and porous materials[17–19]) have been carried out to examine the effects of reduced dimensions, geometrical constraints, and substrate interactions on the orientational ordering. Carefully grown films[20–22] form hcp structures, and the increased ZPM in the outer layers[23] combined with the frustration of the hcp structure apparently prevents long-range ordering, and complete periodic ordering for the molecular orientations has not been observed for these films.

The purpose of this paper is to report studies of the local orientational ordering for (a) thick films (12-layer average) and (b) thin films (bilayers) of hydrogen for ortho concentrations $0.23<X<0.72$ and temperatures $0.05<T<10$ K. In the following sections we will first review the quantum properties of solid hydrogen and the quadrupolar (tensorial) order parameters observed by NMR, and then discuss the experimental work and the results observed.

II. BACKGROUND

The two distinct molecular species of hydrogen (ortho and para) result from the different ways in which the molecular

wave function can be antisymmetrized. The ortho molecules are characterized by an odd rotational quantum number, $J=1,3,5,\ldots$ (total nuclear spin $I=1$) and the para molecules by $J=0,2,4,\ldots$ (with $I=0$). The para-H_2 molecules can be regarded as spherical with only weak van der Waals' interactions. The ortho molecules, on the other hand, have a small axial electric quadrupole moment Q, and they interact via highly anisotropic EQQ interactions with the Hamiltonian[24]

$$H_{\mathrm{EQQ}}^{ij}=\sum_{m,n}\zeta_{mn}(R_{ij})Y_2^m(\omega_i)Y_2^n(\omega_j)Y_4^{m+n*}(\Omega_{ij}), \quad (1)$$

where $\omega_i=\omega_i(\theta_i,\phi_i)$ is the orientation of the ith molecule, Y_2^m is a spherical harmonic in Rose's convention,[25] R_{ij} is the distance between the ith and jth molecules, and $\Omega_{ij}=\Omega_{ij}(\Theta_{ij},\Phi_{ij})$ gives the orientation of R_{ij}. Assuming a rigid lattice and considering only nearest-neighbor interactions, the interaction coefficient ζ_{mn} is given by $\zeta_{mn}=(20\pi/9)(70\pi)^{1/2}\Gamma_{ij}C(224;mn)$ where $C(224;mn)$ is a Clebsch-Gordan coefficient and $\Gamma_{ij}=6e^2Q^2/25R_{ij}^5$ is the nearest-neighbor quadrupole coupling constant. The values of Γ_{ij} for the bulk, and a $\sqrt{3}\times\sqrt{3}$ registered solid on graphite and BN are

$$\Gamma_0=\begin{cases}0.87\ \mathrm{K} & \text{for bulk } H_2\\ 0.528\ \mathrm{K} & \text{for } H_2/\text{graphite}\\ 0.470\ \mathrm{K} & \text{for } H_2/\mathrm{BN}.\end{cases}$$

The lowest-energy configuration for the EQQ interaction is a ''tee'' configuration with molecular axes mutually perpendicular. In any lattice structure other than a simple two-dimensional (2D) square array, the quadrupoles cannot attain the lowest-energy configuration for all pairs because it is impossible for all nearest neighbors to be mutually perpendicular. This feature results from the incompatibility between the lattice geometry and the symmetry properties of the interaction and the system is therefore said to be geometrically frustrated. The phenomenon of frustration [26–33] occurs in a wide variety of apparently disparate systems[34–37] when the competition between interactions does not lead to simple ordered states that are favorable to all interactions, or when there is a fundamental geometrical incompatibility between the symmetry of the interactions and that of the underlying lattice structure (or a combination of both features). The orientational glasses have highly frustrated anisotropic interactions, while purely geometrical frustration[27] occurs for the pyrochlores $Tb_2Mo_2O_7$ (Ref. 38) and $CsNiCrF_6$ (Ref. 39) with antiferromagnetic interactions of spins at vertices of corner-connected tetrahedra. Although the combined effects of frustration and disorder are needed for most glass formers, it is now known that a spin glass ordering can occur without disorder for very strong geometrical frustration [compare the spin glass behavior of the B-spinel $CsNiFeF_5$ (Ref. 40) with the antiferromagnetic ordering of FeF_3 (Ref. 41) for the same lattice structure]. The effects of lattice geometry on frustration are therefore of key importance to understanding the microscopic origins of glass behavior.

The anisotropic intermolecular interactions (principally EQQ) that can lead to admixtures of higher J states in the ground state are weak compared to the separation of the rotational energy levels, and J can therefore be regarded as a good quantum number. In addition, for our experimental temperature range, $k_BT\ll[E(J=3)-E(J=1)]=845$ K, and only the lowest rotational state $J=1$ is thermally populated. Conversion from the $J=1$ state to the $J=0$ state is very slow because it is doubly forbidden (as it requires simultaneous breaking of the spin and orbital symmetries). A wide range of $J=1$ concentrations can be studied by simply aging a sample at low temperatures. The system is therefore an ensemble of strongly interacting spin-1 quantum rotors with a very high degree of frustration. In addition, the rotational degrees of freedom have large zero point motions that will play significant roles in constrained geometries, particularly at free surfaces. Solid hydrogen films can therefore serve as prototype systems for probing the combined effects of disorder and reduced dimensionality on highly frustrated quantum spin systems.

TABLE I. Definition of the operator equivalents ξ^n and Θ^m of the spherical harmonics Y_1^n and Y_2^m, respectively.

	Operator	Moment
Dipole		
	$\xi^0=(1/\sqrt{2})J_z$	$M^0=\langle\xi^{0\dagger}\rangle$
	$\xi^{\pm1}=\mp\frac{1}{2}(J_x\pm iJ_y)$	$M^{\pm1}=\langle\xi^{\pm1}\rangle$
Quadrupole		
	$\Theta^0=1/\sqrt{6}\,(3J_z{}^2-2)$	$Q^0=\langle\Theta^{0\dagger}\rangle$
	$\Theta^{\pm1}=\mp\frac{1}{2}(J_zJ_\pm+J_\pm J_z)$	$Q^{\pm1}=\langle\Theta^{\pm1\dagger}\rangle$
	$\Theta^{\pm2}=\frac{1}{2}(J_\pm J_\pm)$	$Q^{\pm2}=\langle\Theta^{\pm2\dagger}\rangle$

The relevant moments that describe the orientational observables for ortho-H_2 molecules are the expectation values of the operator equivalents of the spherical harmonics in the manifold $J=1$ and are given in Table I. For interacting ortho molecules, we must consider the many-particle crystal wave function in order to account for collective effects that tend to correlate the orientational degrees of freedom of the ortho molecules. The individual molecular states cannot be described in terms of pure states but rather in terms of a single-particle density matrix ρ_i determined by the quadrupole and dipole moments Q_m and M_n, respectively:

$$\rho_i=\frac{1}{3}I_3+\sum_{n=0,\pm1}M_i{}^n\xi_i^n+\sum_{m=0,\pm1,\pm2}Q_i{}^m\Theta_i{}^m, \quad (2)$$

where I_3 is the unit vector. The dipole moments are expected to vanish, and of the five remaining degrees of freedom, three can be used to define local principal axes $(\hat{x}_i,\ \hat{y}_i,\ \hat{z}_i)$ for the quadrupole tensor, leaving only two intrinsic quadrupolar degrees of freedom. These intrinsic degrees of freedom can be represented by two local order parameters, the alignment

$$\sigma_i=-\sqrt{\frac{3}{2}}Q_2{}^0=\left\langle 1-\frac{3}{2}J_{z_i}{}^2\right\rangle \quad (3)$$

and the eccentricity

$$\eta_i=Q_i{}^2+Q_i{}^{-2*}=\langle J_{x_i}{}^2-J_{y_i}{}^2\rangle. \quad (4)$$

As a result of the condition $\mathrm{Tr}\rho^2 \leqslant 1$ these parameters must satisfy the inequality $4\sigma_i^2 + 3\eta_i^2 \leqslant 4$. The allowed values of (σ, η) are then constrained to $-\frac{1}{2} \leqslant \sigma \leqslant 1$ and $|\eta| \leqslant 1 \pm \frac{4}{3}\sigma$.

The NMR line shapes are given by the intramolecular nuclear dipole-dipole interactions, which are directly proportional to the order parameters. The local orientational ordering can therefore be determined by fitting the NMR line shapes to either a fixed order parameter or a distribution of order parameters. This fitting is independent of any assumptions about the lattice structure for the centers of mass of the molecules.

III. EXPERIMENTAL CONSIDERATIONS

Both hexagonal BN and exfoliated graphite (grafoil and papyex) have favorable characteristics for experimental studies of physisorbed films. These characteristics include high homogeneity, large crystal sizes, relatively low corrugation in the substrate potential, and compatibility with different experimental techniques. The lattice spacing of BN is $\sim 2\%$ greater than that of graphite. BN is, however, much more suitable for NMR measurements because its electrical conductivity is much less than that of graphite, and the anisotropic platelet diamagnetism of BN is 40 times less than that of graphite.[42] Powdered forms of BN are commercially available.[43–45] We used BN provided by Johnson-Matthey[45] because their material had the largest surface areas (10–15 m^2/g, compared to 25 m^2/g for graphite[46]).

Careful isotherm studies by Shrestha *et al.*,[47] Evans *et al.*,[48] and Crane *et al.*[49] have demonstrated that BN is a high quality substrate with high homogeneity, large crystallite sizes [0.1–3 μm (Ref. 48)], and relatively low corrugation of the surface potential. A good test of the quality of the substrate preparation is the sharpness of the liquid-solid substep at about 34 torr in the Ar on BN isotherm at 77 K.[50] Although the characterization of the structures of adsorbed systems on BN is not as well known as for graphite, NMR studies have accurately identified the coverage for the commensurate solid ($\sqrt{3}\times\sqrt{3}$) phase for ^{3}He on hexagonal BN, which was 75% of a complete monolayer.[49] Incommensurate structures appear at high coverages. There have been no specific measurements of the density for the $\sqrt{3}\times\sqrt{3}$ registered phase for H_2 on BN, and we assume that it is close to the value for graphite.

The as-delivered samples must be carefully cleaned and annealed prior to any experiment in order to achieve the highest homogeneity and to remove any impurities associated with the manufacturing process. The procedure used is especially critical for surface adsorption studies. While the procedures necessary to produce clean samples have been well established for exfoliated graphite, many different cleaning methods and various heat treatments[51–60] are commonly used for BN powders.

Wolfson *et al.*[61] reported that annealing a BN sample at 900 °C is not always sufficient to produce clean samples and fails to remove soluble borate contaminants (principally boric oxide and boric acid impurities), which would tend to distort the homogeneity of the substrate. In order to remove these impurities, and following the procedure of Shrestha *et al.*[47] we first rapidly rinsed the powder with deionized water, and then washed the samples with methanol. The rate of reaction of BN with water to form boric oxide is extremely slow at 300 K and the water rinse helps to remove the soluble borates. The washing process with methanol was repeated three times, and the BN powder was filtered and dried each time. Small magnetic filings were found after the washing and were carefully removed from the powder samples. It is believed that the filings resulted from the powdering process during manufacturing.

After cleaning, the BN sample was sealed into a 2-in.-diameter quartz tube, which was connected to a low pressure pumping station and placed inside an oven (Thermolyne, Type 21100 Tube Furnace). The sample was outgassed for 4 h at 200 °C and then baked for 24 h at 900 °C under a vacuum of 10^{-6} torr. Samples prepared in this fashion were carefully characterized using adsorption isotherms and from the number of distinct steps observed and the sharpness of the liquid/solid substep in the 77-K Ar isotherm, it was clear that high quality surfaces had been achieved. One concern can be the formation of paramagnetic centers during the baking process. NMR studies are very sensitive to the presence of such centers because they would lead to very significant additional ortho-para conversion rates. In all our cases we found that the conversion rates were significantly slower than those reported for graphite for similar densities. Furthermore, the observed conversion rates appear to vary linearly with the number of layers adsorbed. This would not be the case if there were even moderately low concentrations (e.g., 10 ppm per unit area) of paramagnetic impurities.

The baked BN samples were cooled slowly to room temperature and kept under vacuum until ready to load into a Kel-F NMR sample cell.[62] The BN powder was loaded into the sample cell using a dry-N_2 gas tent, thereby minimizing the exposure to moisture in the atmosphere. It was important to prevent water form adsorbing onto the BN surfaces in order to minimize the ^{1}H background NMR signal. The NMR cell was evacuated with a diffusion pump rapidly after loading with the BN. The BN powder was left as a loose uncompressed sample. In order to make thermal contact with the refrigerator a bundle of fine copper wires was inserted into the powder with one end of the wires soldered to a brass flange. This brass flange was an integral part of a cold finger of a high circulation rate dilution refrigerator. After condensing the sample, a sufficient quantity of ^{4}He gas was introduced into the chamber to completely wet all surfaces in order to improve the thermal contact.

Prior to the NMR studies, we carried out measurements of the partial adsorption isotherms of Ar on BN at 77 K to determine the number of molecules adsorbed per layer. The surface area of the powdered sample was also determined by measuring the volume that had to be admitted for the Ar adsorption at $P \simeq 34$ torr to observe the fluid-solid transition at 1.06 ML.[50] From these measurements and the knowledge of the associated volumes of the H_2 gas handling system, we are able to determine the H_2 coverages to better than 5% for a given volume.

Gaseous H_2 samples of normal ortho-H_2 concentration (75%) were introduced into the sample chamber at about 20 K through a capillary fill line. A bifilar heater wire was wound around the fill line to prevent blockages in the line from solid H_2. We introduced sufficient hydrogen gas to form the layer thicknesses that we wanted to study using the

surface calibrations described above. For the thick films it is not expected that the coverage would be uniform to 12 layers throughout the material, but the condensation was carried out very slowly (over approximately 2 h) to ensure that the coverages would be as uniform as possible. The bilayer coverage was known precisely from the adsorption isotherm studies.[63]

In the preparation of the thick films, capillary condensation can occur with the creation of condensed bulk phases at pressures below the saturated vapor. This occurs in areas of the film where there are large curvatures, and in our case at the edges of the BN platelets. The NMR studies can immediately detect this contribution because the NMR line shapes contributed would match those seen for the bulk phases. As shown in the results in the next section, the NMR line shapes are very different from the bulk line shapes in all ranges of X and T explored, and to within a limit of approximately 5% we can say that we have not seen these contributions.

The NMR absorption signals were observed using a CW NMR quadrature hybrid tee bridge spectrometer operating at 268 MHz.[1] The matched resonant tank circuit is located in the low-temperature region of the dilution refrigerator and is connected to the spectrometer via a 2λ 50-Ω coaxial transmission line of low thermal conductivity. The bridge spectrometer detects the absorptive component of the NMR signal by adjusting room-temperature fine-tuning capacitors so that there is a small unbalance in amplitude between the two arms of the bridge but with no error in phase. The output of the bridge circuit was amplified by a low noise room-temperature narrow-band rf receiver, and the signal voltage modulating the carrier is detected by an rf mixer. The spectra were recorded by sweeping the magnetic field through the resonance with simultaneous ac modulation (1 G) and lock-in detection. The magnetic field sweep and lock-in amplifier output were interfaced via a IEEE 488 bus to a personal computer using a National Instrument AT-MIO-16H-25 digital-to-analog conversion board (DAC) for automated data acquisition. The data acquisition system allows continuous data collections 24 h a day except during liquid helium transfers.

To reduce spurious ^{1}H background NMR signals from being introduced into the proton NMR line shapes, the sample chamber was constructed from Kel-F, which is known to have a negligible proton content. However, as a result of the enhanced sensitivity of our spectrometer, we did, however, detect a small residual background signal. Figure 1(a) illustrates a typical derivative NMR line shape for the residual background signal. The shape of the background signal remained constant over the entire temperature range studied, indicating that there was only one source for the background signal. Figure 1(b) shows a typical derivative NMR absorption line shape of H_2/BN that includes the background signal. The line shapes arising from the molecular hydrogen were therefore determined by subtracting the fixed background signal, which was measured under the same conditions without H_2 present.

The NMR line shapes presented here represent the average of a single up and down sweep. The sample temperatures reported are the average of the initial and final temperatures for each down and up sweep. Data analysis programs were written using MATHEMATICA (Ref. 64) in order to subtract background spectra and integrate the line shapes for presentation as functions of ortho concentration and temperature.

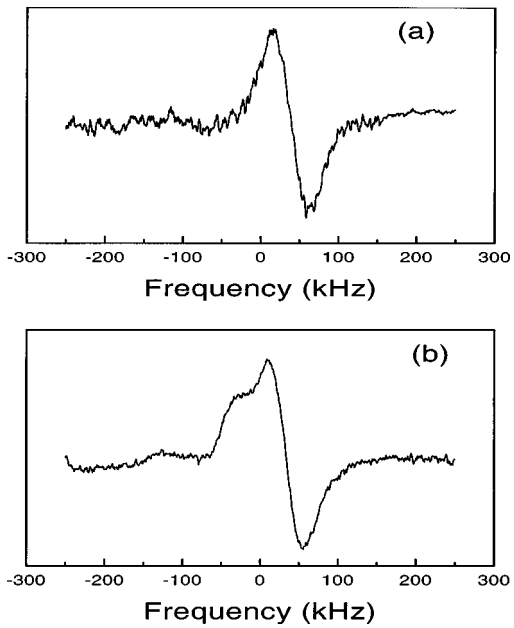

FIG. 1. Typical NMR line shapes observed for H_2 on BN at 1 K for (a) only the proton background signal and (b) for both the hydrogen film and proton background.

IV. 12-LAYER FILMS

A. Experimental results

In this section, we present averaged derivative and integrated CW NMR absorption line shapes observed for 12-layer films of H_2 on BN as functions of temperature and ortho concentration. The ortho concentrations of aged samples were determined by comparing the total NMR absorption signal amplitudes measured at a standard reference temperature (4.2 K). Using these measurements, the ortho-para conversion for the full film was best fitted by a bimolecular decay process with a conversion rate of 1.43 $\pm$0.005%/h. This is less than the bulk value of 1.9%/h but greater than the value (0.9%/h) observed for the 8-layer film coverages previously reported.[6]

The NMR line shapes observed were distinctly different from the line shapes observed previously, either for bulk H_2 (Ref. 65) or in 2D monolayers,[5] for all concentrations and temperatures explored, except for the trivial rotationally disordered line shape observed for high temperatures. (A comparison of the line shapes observed for bulk H_2, monolayers and thick films is given in Fig. 2). Three distinct line shapes corresponding to different orientational ordering regimes were observed: (I) an orientationally disordered [Gaussian line shape, $\sim$50 kHz full width at half maximum (FWHM)]; (II) a mixed phase with order and disorder coexisting with a two-component line shape consisting of a central Gaussian component plus a wing structure with peaks at ($\pm$)150–170 kHz; and (III) a state with strong orientational ordering plus quadrupolar glass ordering with a line shape showing a double peak in the outer wings. (The three classes of NMR line shapes are shown in Fig. 3.)

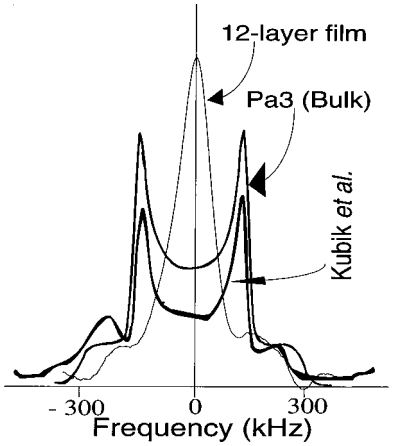

FIG. 2. Comparison of the low temperature NMR spectra observed for Pa3 ordering in bulk samples of solid H_2 (Ref. [65]), pinwheel ordering of H_2 on Grafoil (Ref. 5), and 12-layer films of H_2 on BN (this report).

Regime III is seen at the lowest temperatures, $T \leqslant 0.25$ K for $0.45 < X < 0.65$ and $T \leqslant 0.7$ K for $0.25 < X < 0.45$. Region II is observed for intermediate temperatures. No line shapes intermediate between those of region II and region III could be clearly distinguished, and transitions of one line shape to the other occurred at well defined temperatures. We therefore identify three classes of orientational ordering for thick films

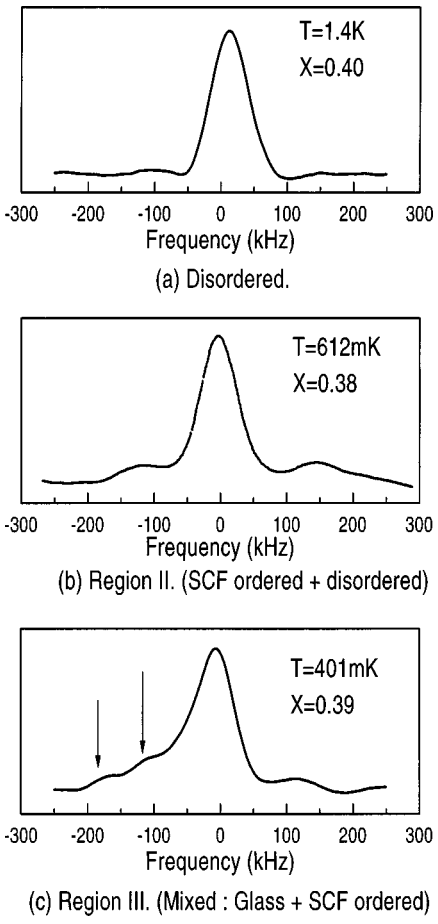

FIG. 3. Three classes of NMR line shapes observed for 12-layer films of H_2 on BN.

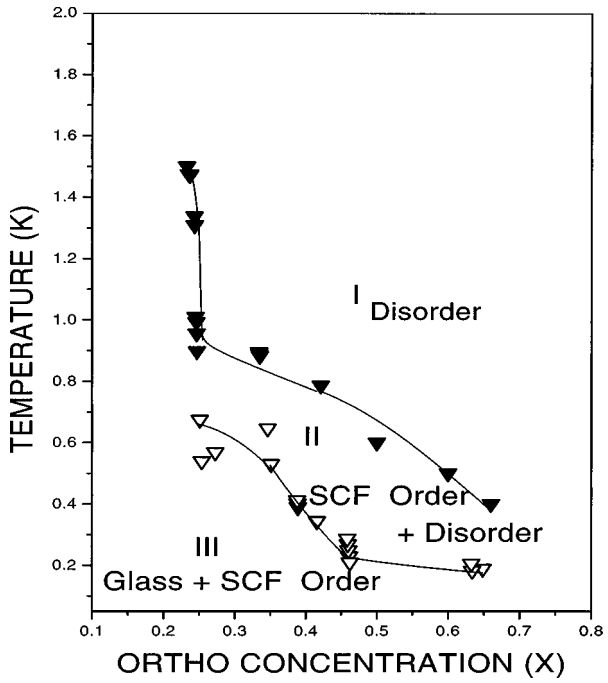

FIG. 4. Phase diagram for thick (12-layer) films of H_2 on BN as inferred from NMR studies. (The solid lines are guides to the eye only.) The symbols represent the observed changes in the NMR line shapes, and SCF designates substrate crystal-field ordering.

that define distinct regions of the (X,T) phase diagram for this system (Fig. 4). This phase diagram is distinctly different from that observed for bulk samples or for monolayers of H_2 on graphite.

Typical CW NMR derivative and integrated absorption line shapes characteristic of regime II of the phase diagram are shown in Fig. 5. The main features of the line shapes are a strong central Gaussian peak (FWHM of 58 ± 2 kHz) and the appearance of a component that is close to 100% orientationally ordered as evidenced by the formation of two wing structures separated by approximately 320 ± 5 kHz. The wings begin to appear for ortho concentrations $X \leqslant 0.66$ and temperatures $T \leqslant 0.4$ K. The fact that significant orientational ordering is not observed for high ortho concentrations ($X > 0.66$) even at temperatures as low as 0.1 K is in strong contrast to the behavior observed for bulk samples. This property for films is believed to result from the competition between the substrate interactions and the short-range EQQ interactions. The latter are reduced significantly at the free surface of the film because of the large zero-point fluctuations of the orientations. This is discussed in the next section.

If one subtracts the central Gaussian from the line shape, the outer wings of the NMR line shape can be fitted to a Pake doublet line shape, corresponding to orientationally ordered molecules with a well-defined mean local order parameter $\bar{\sigma}$. For Fig. 5(b) the fit yields $\bar{\sigma} = 0.86 \pm 0.08$. As the concentration X decreases the outer wings increase in amplitude at the expense of the central disordered peak.

The transitions of the wing structure in moving from region I to region II of the phase diagram are reasonably sharp (e.g., $T_c = 0.90 \pm 0.05$ K for $X = 0.4$) but we could not identify a true first-order phase transition with hysteresis at this boundary. In region II of the phase diagram, $\bar{\sigma}$ increases as

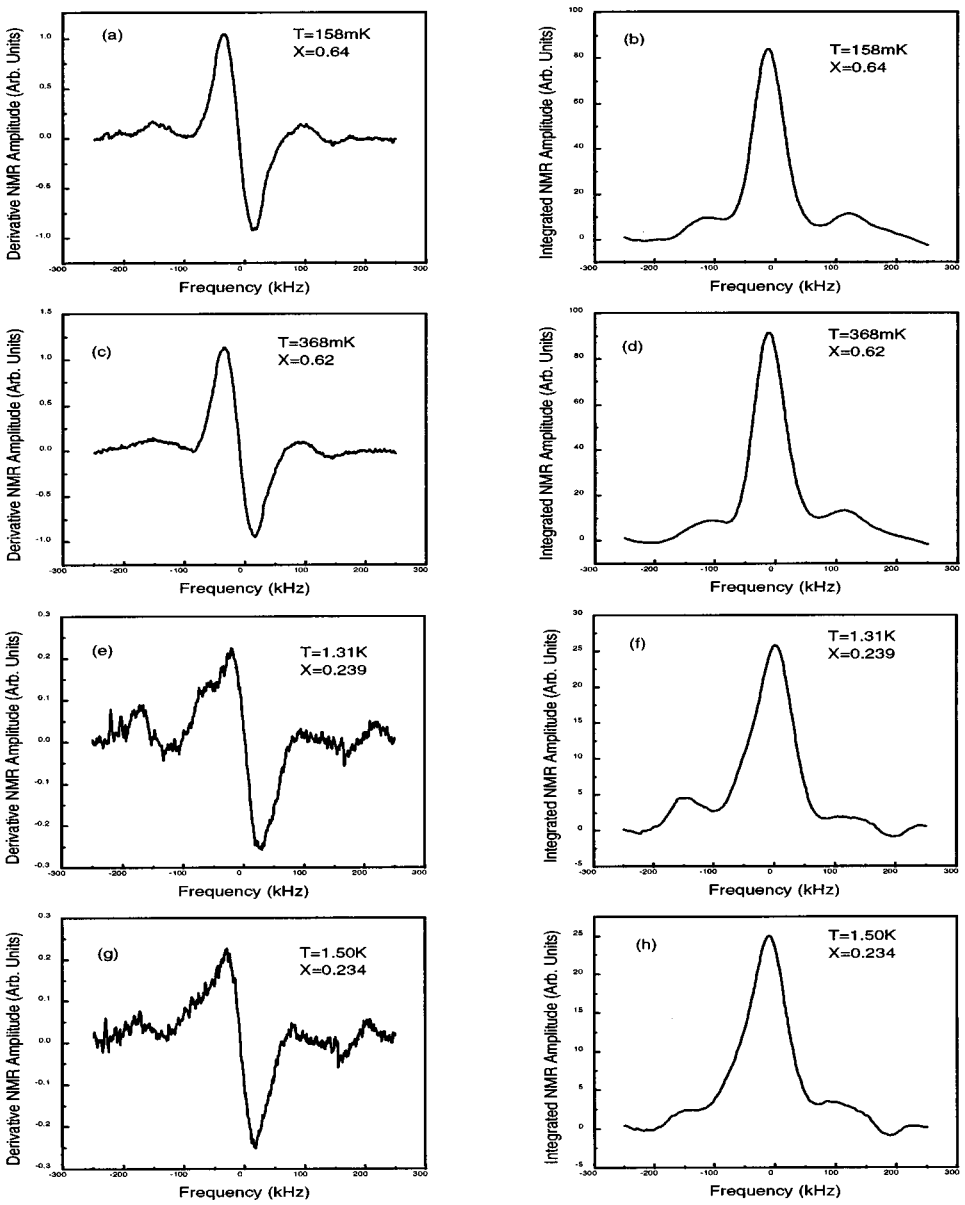

FIG. 5. Typical CW NMR derivative and integrated absorption line shapes for region II of the phase diagram for 12-layer H_2 films on BN: mixed SCF ordered and disordered states.

the temperature is reduced. This growth of the local orientational order is similar to the behavior observed for bulk H_2 but for totally different values of X and T. The intensity (i.e., height and area) of the wing structures also increases at the expense of the amplitude of the central peak as $\bar{\sigma}$ increases. This is in contrast to the report of NMR studies for thin films (4 and 8 layers).[6]

The behavior for region II can be understood quantitatively if the orientational ordering occurs predominantly in the first 2–3 layers near the BN substrate for the temperature range explored. (In the studies of 4- and 8-layer films, it was shown that the orientational ordering occurred principally in the first four layers.[6]) The temperature dependence of the wing components of the line shapes is well described by a temperature-dependent $\bar{\sigma}$ given by a constant crystal field V_c. The detailed analysis is given in Sec. IV B. The ordering is therefore driven principally by the anisotropic interactions with the substrate, which is therefore referred to as a surface crystal field (SCF) ordering. The basic NMR line shape of region II, consisting of a central Gaussian plus well-defined wings given by $\sigma(T)$, extends down to low concentrations without any significant changes [Figs. 5(e)–5(h)].

At the lowest temperatures explored the NMR line shapes were observed to transit to a completely new structure. This is labeled as region III in the phase diagram of Fig. 4. The new line shapes of this region are plotted in Fig. 6, and are characterized by the emergence of clear double peaks (marked by A and B) in the outer wings. The peak component marked B resembles the features observed for the quadrupolar glass line shapes seen for bulk H_2 samples for intermediate ortho concentrations.

In order to test this interpretation we fitted the B component to a glass line shape using a broad order parameter distribution $P(\sigma)$. The fit to the line shapes is shown in Figs. 7(a) and 7(c). The weighting of the components was made by assuming that the number of molecules contributing to the

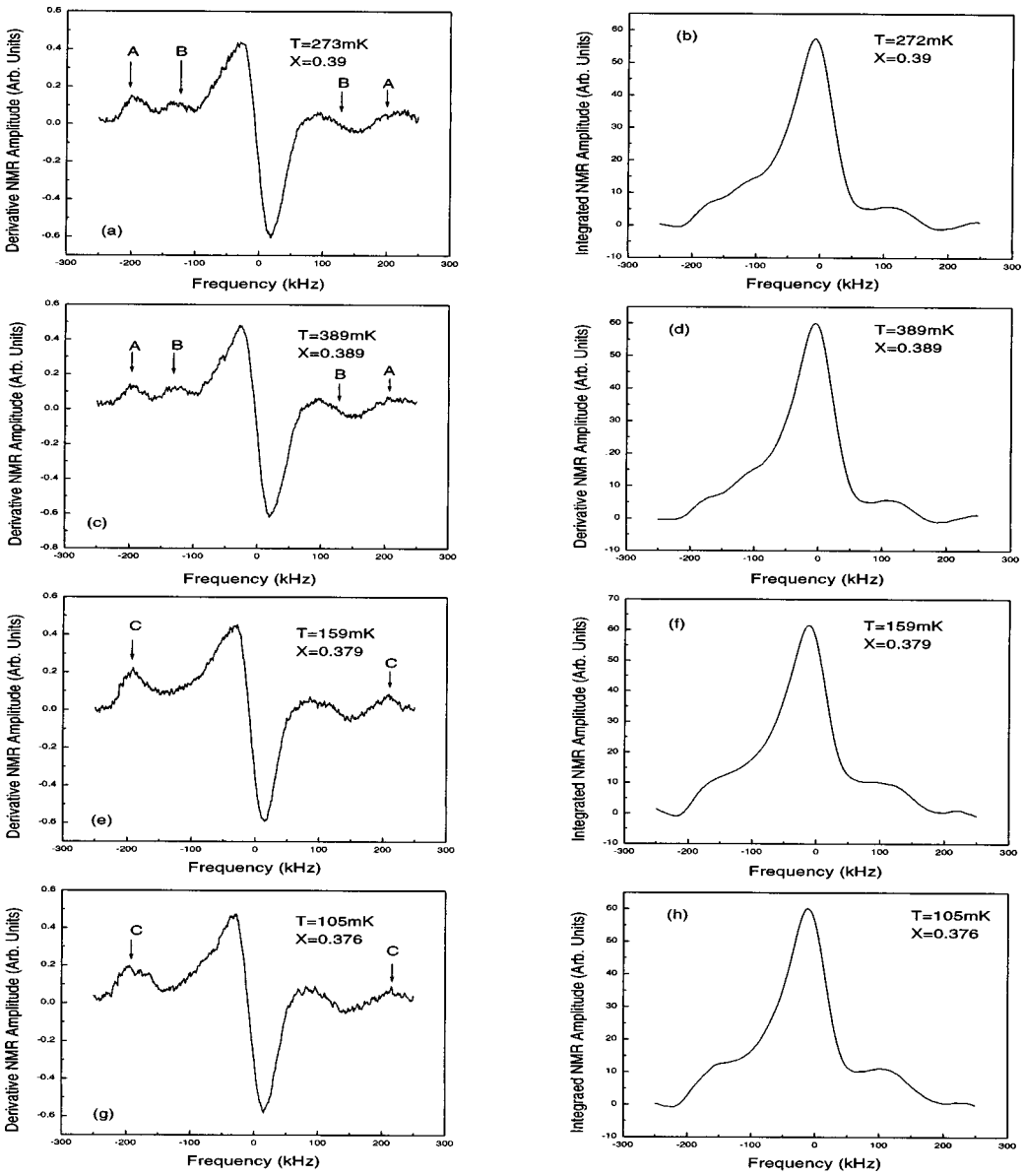

FIG. 6. Typical CW NMR derivative and integrated absorption line shapes for region III of the phase diagram for 12-layer films of H_2 on BN: mixed quadrupolar glass and SCF ordered states.

three features remained approximately constant. At the lowest temperatures, $P(\sigma)$ develops the characteristic triangular distribution of the glass state, and the B feature shifts to $\overline{\sigma} \sim 0.8$–$0.9$ and finally merges with the C feature at very low temperatures [Figs. 6(e) and 6(g)]. The temperature dependence of the evolution of $P(\sigma)$ is smooth and very similar to that observed for the bulk hydrogen quadrupolar glass state but for different ortho concentration and temperature ranges. It should be noted that the line shapes in Fig. 6 are not symmetric with respect to the center of the absorption spectrum. This is believed to be the difficulty in accurately subtracting the background spectrum that occurs on the high-frequency side of the spectrum.

We have therefore interpreted the line shapes in region III in terms of three components that arise from different parts of the films: (i) a central disordered line attributed to the outer layers, (ii) a quadrupolar glass line shape (with outer edges in the spectrum at position B) attributed to the intermediate layers, and (iii) a line shape component showing almost complete orientational ordering (with wings extending out to position A) and attributed to the influence of the substrate interactions on molecules near the substrate. (A detailed discussion of the fit is given in the following section.)

The invariance of the central disordered component of the line shape to the variations in temperature and ortho concentration is most remarkable. We can only understand this if the molecules in the outer layers near the free surface remain disordered down to the lowest temperatures studied. This behavior is attributed to the enhanced ZPM in the outer layers, which inhibits the orientational ordering. Clearly this interpretation does not depend on uncertainities in the thickness of the films. It is interesting to note that just the opposite behavior would be expected from any bulklike phases on the substrate, such as those generated by capillary condensation.

The orientational properties of the film as a function of concentration is quite unexpected. Below $X = 0.25$ the transitions to the disordered phase (region I of the phase diagram) occur at much higher temperatures. Furthermore, the

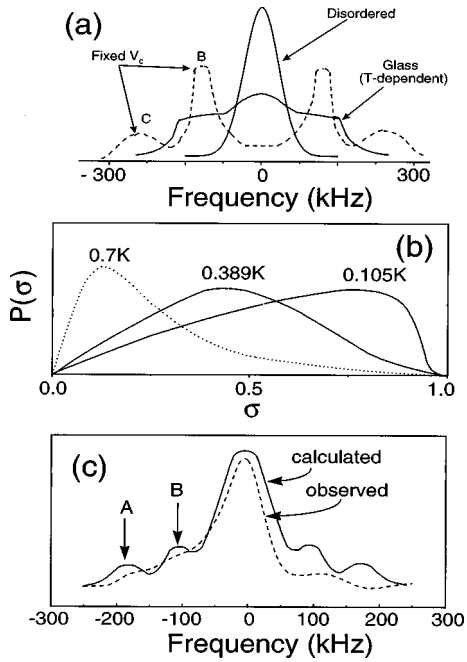

FIG. 7. (a) A schematic interpretation of the three-component NMR line shape in the low-temperature, low-concentration regime of the phase diagram for 12-layer films, (b) the corresponding order parameter distributions for the glass component, and (c) comparison of the calculated line shape [sum of components in (a)] with the experimental line shape.

outer wings of the NMR spectra increase their separation, corresponding to an increasing σ. For example, for $X \leqslant 0.25$, the separation of the outer wings is approximately 380 ± 7 kHz, and the width of the central Gaussian increases to 80 ± 5 kHz. This behavior contrasts strongly with that observed for bulk samples where the orientational order parameters decrease as X is reduced. This behavior for low X in thick films results from the competition between the collective EQQ interactions and the strong substrate (or anisotropic local crystal field) interactions. The EQQ interactions oppose the SCF-ordering (i.e., aligned parallel to the local symmetry plane of the substrate), and the effects of the EQQ interactions become very weak as one approaches the percolation concentration $X \simeq 0.15$.

B. Analysis

In the qualitative interpretation presented above, we proposed that orientational ordering in the layers nearest the substrate was initially driven by a relatively strong anisotropic substrate interaction

$$H_{c_i} = V_c (J_{z_i}^2 - \tfrac{2}{3}). \tag{5}$$

For $V_c > 0$, the single-particle substrate field will lead to a quenched rotational state in which the molecules will tend to align parallel to the $\hat{z}$ axis (normal to the substrate). For $V_c < 0$, the independent particle solution is a planar rotor with molecular axes perpendicular to $\hat{z}$ (i.e., parallel to the plane of the substrate).

If $|V_c| > |H_{\mathrm{QQ}}| \simeq 1$ K, the substrate fields will orient the molecules adjacent to the substrate surfaces, and this will propagate to at most one layer of neighboring molecules via the anisotropic EQQ interactions. The latter, because of their geometrical frustration, will oppose the ferromagnetic ordering tendency of H_{c_i}, and in a first approximation, the two competing interactions can be represented by a mean-field interaction which leads to a temperature-dependent gap $\Delta(T)$ between the $m_J = 0$ and $m_J = \pm 1$ states with

$$\Delta_i(T) = V_c - \tfrac{27}{2} \Gamma \sigma_i(T). \tag{6}$$

It is this partial lifting of the degeneracy of the m_J states for molecules near the surface that leads to the appreciable values of σ that are associated with the wing structures in the NMR spectra at $\delta\nu = 300$–400 kHz (Figs. 5 and 6). The fact that the remainder of the NMR line shapes retain the Gaussian shape associated with disordered molecules leads us to conclude that the bulk of the film (the ~ 10 layers near the free surface) remain rotationally disordered ($|\sigma| < 0.2$) down to 100 mK for the ortho concentrations we have explored. We now consider this model for the orientational ordering quantitatively in terms of the NMR line shapes calculated for ordering induced by the substrate crystal field interactions in competition with the EQQ interactions.

We first consider the low-concentration/low-temperature regime III of the phase diagram. The unique feature of the spectra of this region is the distinctive double-peak structure in the outer wings (A and B of Fig. 7). Feature B moves toward A continuously on lowering the temperature and A and B merge as a single peak identified as C in Fig. 7. The position of A moves smoothly on raising the temperature from 402 ± 2 kHz at 0.05 K until it reaches 350 ± 5 kHz at $T \simeq 0.38$ K where the apparent transition to regime II of the phase diagram occurs.

The fact that the wing structure occurs at $\delta\nu = +201$ kHz and $\delta\nu = -201$ kHz with a total separation $\nu_{AA} = 402$ kHz clearly indicates that the spin-orbit interaction $H_{\mathrm{SO}} = -c\vec{I}\cdot\vec{J}$ with $c = 113.9$ kHz plays a major role in determining the NMR line shape. If J_z were fully quenched ($\langle J_z \rangle = 0$) the maximum separation that could be produced by the intramolecular dipole-dipole interactions is $6D|\sigma| = 346|\sigma|$ kHz. Even with maximum values for $|\sigma| = 1$ (which is most unlikely at dilute ortho concentrations) the spectra observed cannot be described without considering H_{SO} with $\langle J_z \rangle \neq 0$.

The NMR spectra expected for partially quenched rotors has been considered in detail by Reif and Purcell[66] and by Dubault and Legrand.[67] Typical calculated spectra are shown in Fig. 7(c). The outer wings occur at $\delta\nu = \pm(c - 3d\sigma)$. [Note that in the notation of Dubault and Legrand, the order parameter $R = \langle 3\cos^2\theta - 1 \rangle = \frac{4}{5}\sigma$ and the crystal field $H_c = A(3\cos^2\theta - 1)$ becomes $H_c = -(6A/5)(J_z^2 - \frac{2}{3})$, using the operator equivalence $(3\cos^2\theta - 1) \equiv -\frac{2}{5}(3J_z^2 - J^2)$ in the manifold $J = 1$.]

For $V_c < 0$ (i.e., $A > 0$), the $m_J = \pm 1$ states lie below the $m_J = 0$ state (with a gap Δ), and considering H_c alone, σ is negative, with a low-temperature limit of $\sigma = -\frac{1}{2}$. The outer peak separation therefore becomes $\nu_{AA} = 228 + 346|\sigma| = 401$ kHz at $|\sigma_{\max}| = +\frac{1}{2}$. The very close agreement of this calculated value with the observed values for ν_{AA} at the lowest temperatures is a strong indication of the correctness of the model proposed for the orientational ordering in the NMR

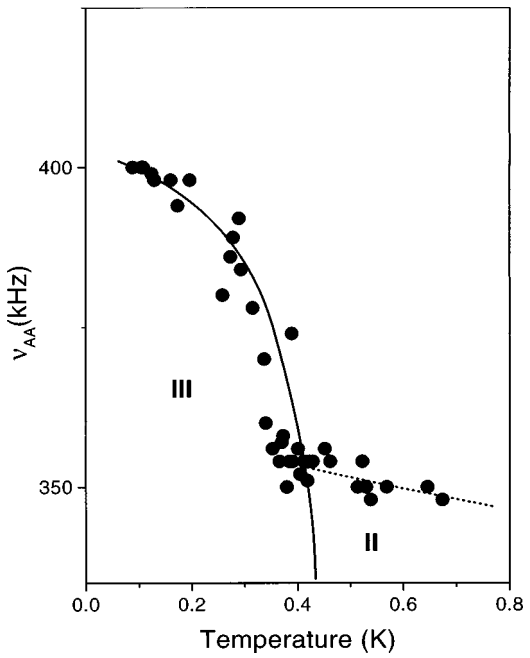

FIG. 8. The temperature dependence of the separation of the outer peaks A of the NMR spectra in regime III of the phase diagram for 12-layer films of H_2 on BN. The solid line shows the best fit for a crystal field $V_c \simeq -2.45$ K.

wings. For $V_c > 0$ (i.e., $A < 0$), Dubault and Legrand[67] show that the calculated spectra are Pake-doublet line shapes with a maximum wing peak separation $\nu_{AA} = 6d\sigma$. This value does not fit the spectra observed, and we conclude that for H_2 on BN, V_c is negative.

We can determine the magnitude of V_c from the temperature dependence of ν_{AA} (regime III of Fig. 4). The order parameter

$$\sigma_i = \langle 1 - \tfrac{3}{2} J_{z_i}^2 \rangle = \tfrac{3}{2}(P_{0_i} - \tfrac{1}{3}), \tag{7}$$

where P_{0_i} is the thermal population of the $m_J = 0$ state for the ith molecule

$$P_{0_i} = e^{-\Delta_i / k_B T} / (2 + e^{-\Delta_i / k_B T}) \tag{8}$$

for an energy gap Δ_i. We therefore have

$$\sigma_i = 1 - 3/(2 + e^{-\Delta_i / k_B T}), \tag{9}$$

where

$$\Delta_i = V_{c_i} - \tfrac{27}{2} \Gamma \sigma_i(T). \tag{10}$$

$\sigma(T)$ can be determined from the expression

$$\nu_{AA}(T) = 228 + 346 |\sigma(T)| \tag{11}$$

and Eq. (11) is then used to determine V_{c_i}. The fit shown by the solid line in Fig. 8 is given by $V_{c_i} = -2.45$ K. This is to be compared with the value $|V_c| = 0.65$ K for H_2 on graphite determined by Kubik *et al.*[5] and the value of $|V_c| \simeq 30$ K estimated by Novaco and Wroblewski.[68] The value of $|V_c|$ for bulk H_2 is $\simeq 0.02$ K.[69]

The above analysis gives a good quantitative description of the outer peak structure ν_{AA} (region III of the phase diagram) in terms of the orientational ordering driven by the substrate crystal field. At the transition to region II of the phase diagram, the temperature dependence changes dramatically (Fig. 8). The temperature dependence is now quite weak with $\nu_{AA} \simeq 345$ kHz at the lowest value and is comparable to the values expected for a bulk Pake-doublet ordering due to orientationally ordered molecules for 3D rotors with $\nu_{DD}|_{\max} = 346\sigma$. The relative sharpness of the outer wings leads us to conclude that there is not a large distribution of order parameters in this regime as there is for the quadrupolar glass phase for bulk samples. This is not true for the B feature of the spectra seen only in region II of the phase diagram. As discussed in detail above, this feature is best fitted by a broad distribution of order parameters that is the signature of the quadrupolar glass. Region III of the phase diagram is therefore interpreted as a mixture of a substrate crystal-field-induced ordering (principally the first layer) plus a quadrupolar glass structure (at most two layers above the first layer), with the remainder of the film remaining disordered (the large central Gaussian line shape). This model for the ordering at the lowest temperatures is illustrated schematically in Fig. 9.

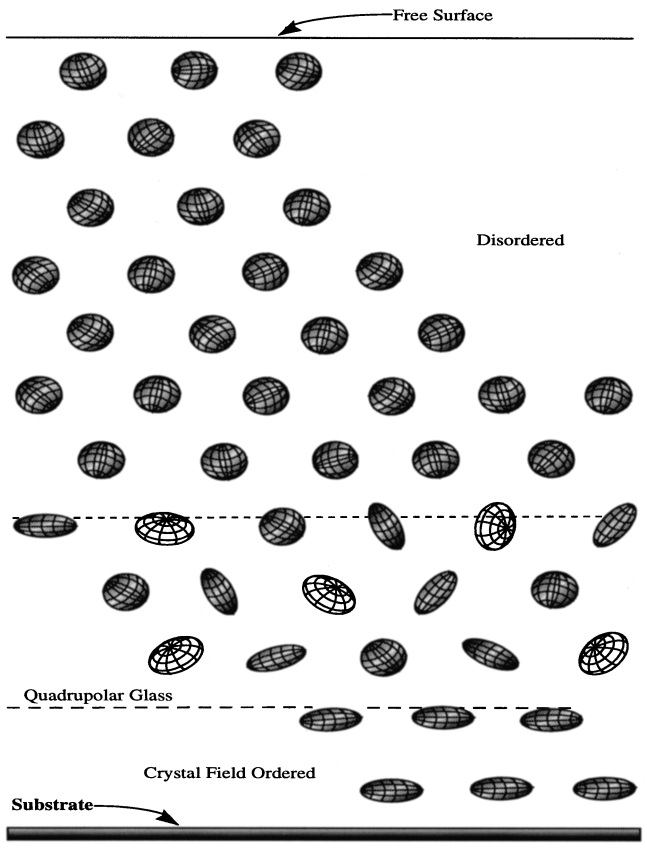

FIG. 9. Schematic representation of the low-temperature orientational ordering in thick films of H_2 on BN, as inferred from the NMR studies.

V. BILAYER FILMS

A. Experimental results

Five distinct NMR line shapes were observed for the bilayer films and their detailed shapes and occurrences as functions of temperature and ortho concentration are different

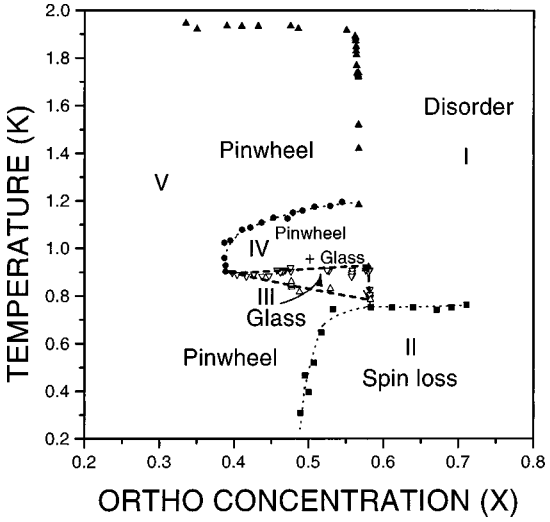

FIG. 10. The phase diagram for bilayer films of quantum rotors on BN inferred from NMR studies.

from both the bulk line shapes and those discussed above for thick films. The phase diagram for bilayer films deduced from the changes in the NMR line shapes is shown in Fig. 10. The five classes of line shapes defining the different regions of the phase diagram are (I) a featureless narrow Gaussian line shape for the rotationally disordered phase, (II) an unidentified structure characterized by an appreciable ''loss'' of nuclear magnetization as evidenced by a strong deviation from the nuclear spin Curie law, (III) a quadrupolar glass state, (IV) a region with coexisting long-range orientational ordering and glass ordering, and (V) pure long-range orientational ordering. The NMR line shapes are very different for the disordered, glass, and long-range (e.g., pinwheel) orientational ordering, making these identifications straightforward. The long-range orientational ordering associated with a fit of the line shapes to a unique σ is expected to be a pinwheel ordering based on the predictions of the theoretical models. NMR alone cannot distinguish between pinwheel and herringbone structures for a powdered sample, and detailed scattering studies are needed to confirm the identification of the long-range ordering. The interpretation of the NMR line shapes in terms of a unique σ or a very small distribution, $P(\sigma)$, is independent of any assumptions about the underlying lattice structure.

The most puzzling feature is the apparent loss of spin magnetization ($\sim 60\%$) in region II of the phase diagram, for ortho concentrations $0.52 \leqslant X < 0.7$ and temperatures $T \leqslant 0.7$ K. Figure 11(a) depicts the spectrum for this ''spin-loss'' region. This strikingly narrow NMR line characteristic of the spin loss region changes abruptly near $X \sim 0.50$ to the ordered line shapes. A strong departure from Curie's law for the $I=1$ spins has also been reported by Clarkson *et al.*[71] and by Cochran *et al.*[72] for bulk systems. There is no theory to explain this ''spin-loss'' effect. The phenomenon may be related to the observations of Chen and Slichter[73] in experiments where large local fields produced by a fraction of spins resulted in a very short nuclear spin-spin relaxation time, T_2, preventing observation of those spins with their spectrometer. However, we believe that the $I=1$ spin loss in the H_2 systems is associated with the saturation of the NMR lines for spins with exceptionally long T_1 times. It is well known

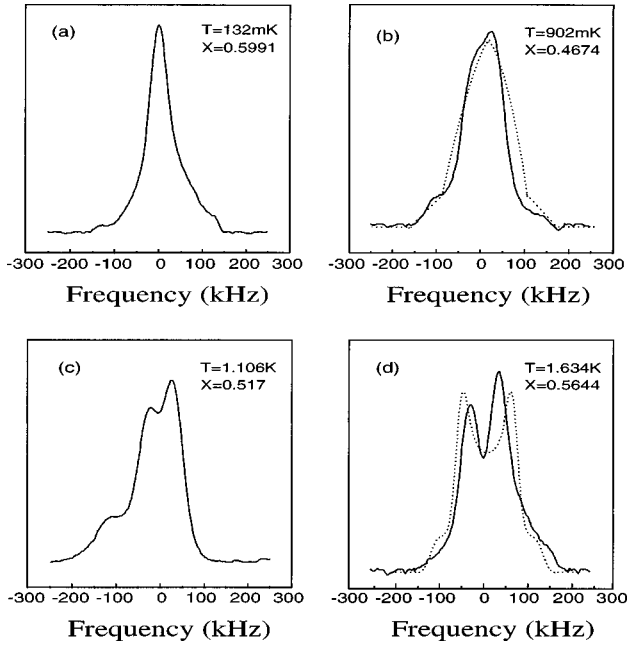

FIG. 11. The different types of NMR spectra observed for bilayers of H_2 on BN: (a) the spin loss regime, (b) the quadrupolar glass state, (c) the coexisting long-range order (expected pinwheel) plus quadrupolar glass state, and (d) the purely long-range ordered regime (expected pinwheel). The dotted lines in (b) and (d) refer to calculated fits to the NMR line shapes for the short-range glass and long-range ordering ($\sigma = \text{const}$), respectively.

that in the ordered phases (glass or long-range ordering), $T_1^{-1} \propto (1-\sigma)$, and molecules with values of $\sigma \simeq 1$ have much longer relaxation times than other molecules. In order to test this explanation, we carried out NMR measurements with different low rf levels varying from -20 dBm to -30 dBm. Partial recovery of the ''lost'' spins was observed, but a fully satisfactory quantitative explanation was not obtained.

The quadrupolar glass regime (II) occurred for ortho concentrations $0.4 \leqslant X \leqslant 0.59$ and temperatures $0.76 \leqslant T \leqslant 0.91$ K. This region is characterized by a broad distribu-

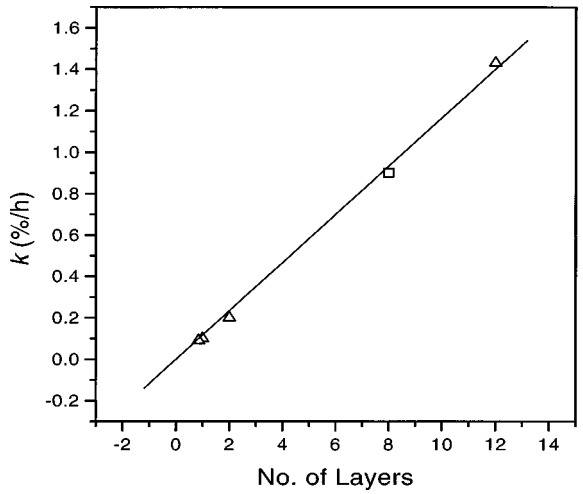

FIG. 12. The ortho-para conversion rate k as a function of the number of layers of H_2 on BN. Note that the conversion rate for 8-layer films of H_2 on BN (square symbol) is from Ref. 6.

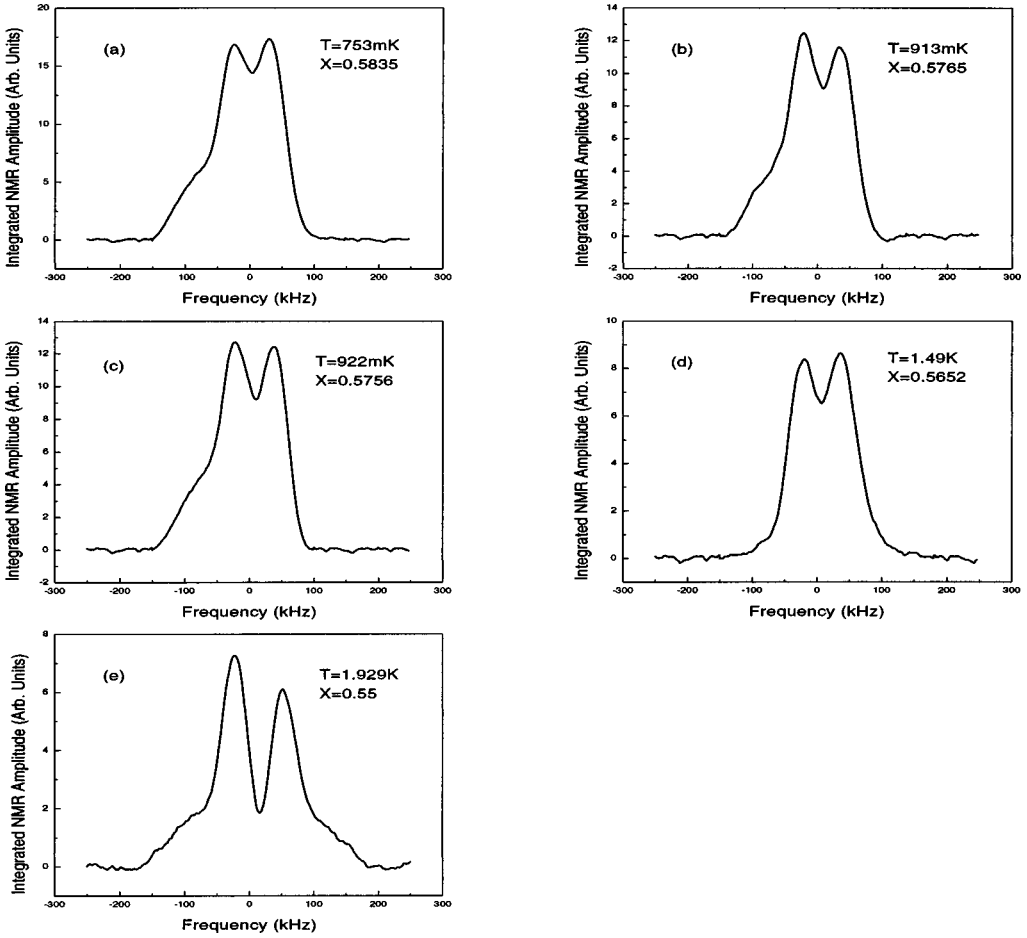

FIG. 13. Observed CW NMR integrated absorption line shapes in region V of the phase diagram for bilayers of H_2 on BN. These line shapes correspond to long-range ordering (expected pinwheel) for ortho concentrations $0.55 \leqslant X < 0.6$. Note that (a)–(c) come from the border line of region V in the phase diagram.

tion of local order parameters. The broken line in Fig. 11(b) shows the best fit for $P(\sigma) \simeq \sigma$. The transitions to the quadrupolar glass state are continuous but occur over a relatively narrow tem-perature range and are represented by ''open and down'' triangles in the phase diagram. This orientational quadrupolar glass disappears at $X \simeq 0.38$.

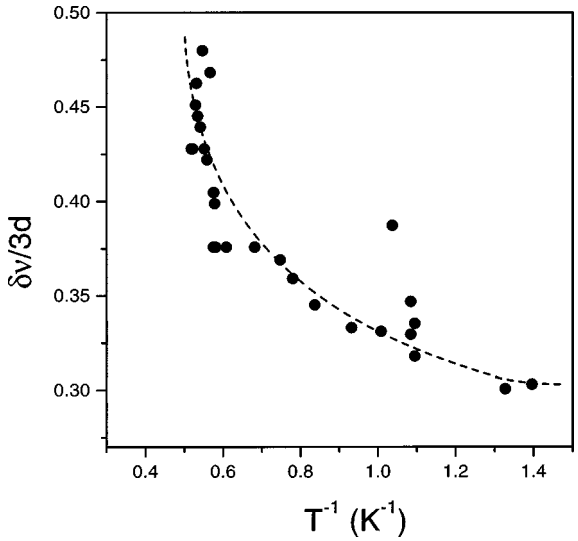

FIG. 14. Temperature dependence of separation of peaks of NMR spectra associated with long-range ordering in the first layer of bilayer films. The dashed line is a fit for a substrate interaction $V_c = -1.25$ K.

For temperatures above those for which the glass state occurs, we observe a mixed state (region IV) with coexisting long-range order (corresponding to $\sigma \sim 1$) plus a component showing quadrupolar glass ordering at the same ortho concentrations. The NMR line shape characteristic of this regime is shown in Fig. 11(c). The glass states are only observed for a central region of the (X,T) phase diagram ($0.75 < T < 1.2$ K and $0.4 < X < 0.6$). Outside this region we observe line shapes characterized by a unique value of σ and thus *only* attributable to long-range orientational ordering [Fig. 11(d)]. This region V of the phase diagram could be a pinwheel or herringbone ordering, but we expect a pinwheel ordering based on the predictions reported for 2D Monte Carlo simulations.[74]

Using the intensity of the integrated NMR signals and the independent measurements of the temperature, we could determine the ortho concentration and thus the ortho-para conversion rate in the bilayer films. The conversion for the bilayer films was best fitted by a bimolecular decay process with a conversion rate of $0.200 \pm 0.007\%$/h. This rate is much lower than the bulk values because of the reduced number of intermolecular magnetic interactions responsible for the conversion. This conversion rate observed for H_2 on BN is slower by a factor of two than that observed for H_2 on

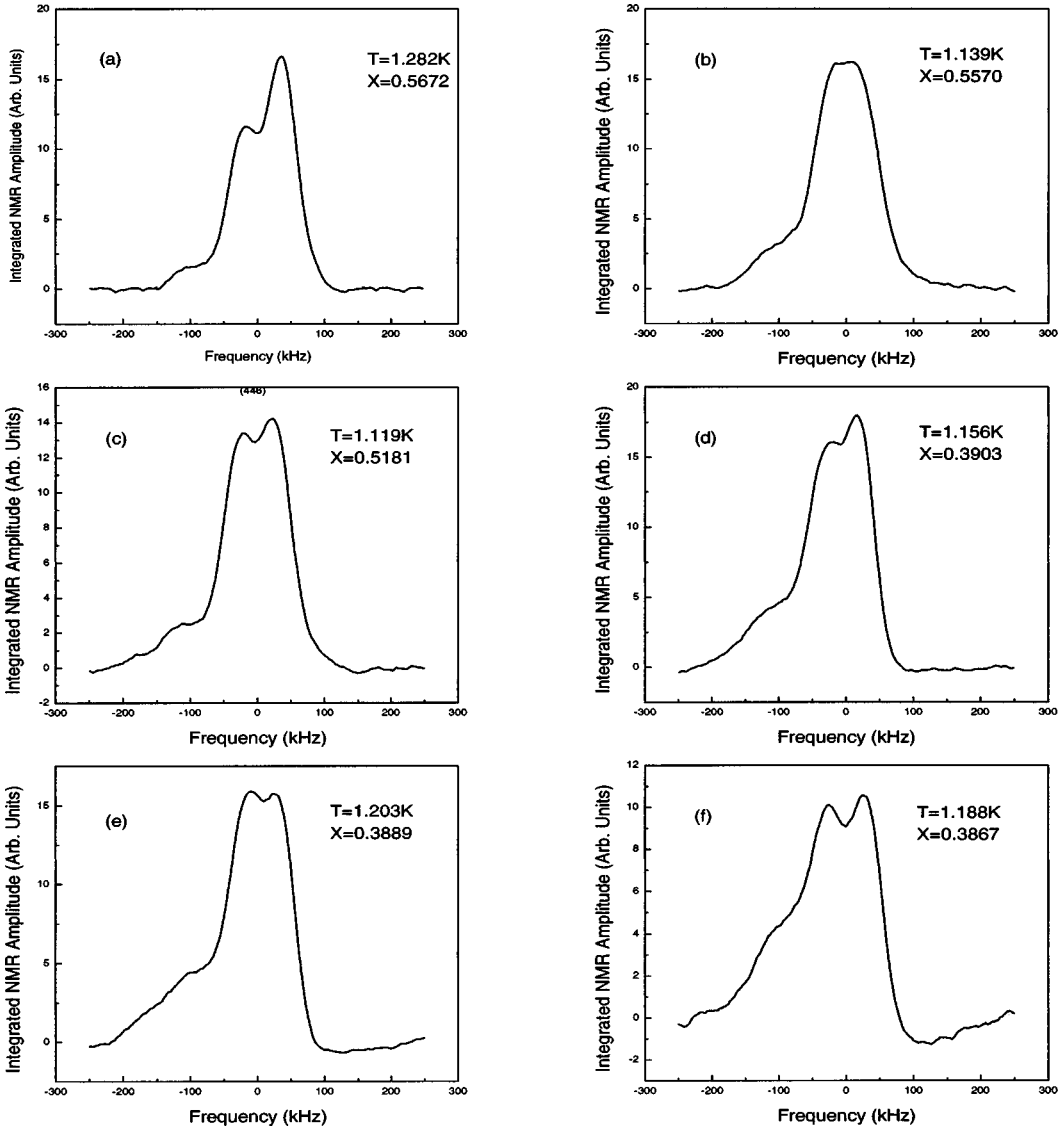

FIG. 15. The NMR line shape for region IV of the phase diagram for bilayers of H_2 on BN. The line shapes correspond to a mixed state with coexisting quadrupolar glass and long-range orientational ordering.

Grafoil (0.4%/h).[5] In Fig. 12, the conversion rate per layer is plotted for both the bilayer and thick films of this study and compared to the rates reported for monolayers on graphite and for bulk H_2. It appears that the conversion rate per layer is linearly dependent on the layer coverage. The slope of the fit in Fig. 12 is $0.116 \pm 0.002\%/\mathrm{h}$ per layer.

B. Discussion

Hydrogen films on BN are expected to exhibit strong layering effects, following observations on similar systems. The second layer in bilayer films of H_2 or D_2 adsorbed on MgO or graphite reveals 2D phases similar to those observed in 3D with much lower temperature liquid-vapor critical and solid-liquid-vapor triple points.[75,76] Ma *et al.*[76] had observed layer-by-layer growth of H_2 on MgO until six steps were measurable at 8.88 K. In particular, they observed that a film of somewhat greater than two layers may exhibit a strong anomaly in orientational ordering. In the bilayer films the first layer is expected to form a compressed triangular lattice and the second layer a solid of unknown lattice structure. It may be possible that this anomaly is associated with the EQQ interactions between molecules in each layer and the combined effects of the EQQ interactions between the layers and the interactions, V_c, with the substrate. NMR studies can be used to probe this interlayer interaction on the orientational ordering. The substrate is expected to modify the orientational ordering in the second layer. It has been proposed[77] that heat capacity measurements of ^{3}He on graphite can be interpreted in terms of a triangular second-layer solid having $\sqrt{7}\times\sqrt{7}$ registry with respect to the first adsorbed layer. For the case of hydrogen, the second layer in the bilayer films of H_2 adsorbed on BN may also form a $\sqrt{7}\times\sqrt{7}$ incommensurate structure with respect to the first adsorbed layer, but this has not been demonstrated. The second and higher layers are only weakly influenced by the substrate and are therefore expected to undergo orientational ordering induced by the EQQ interactions. In the case of coverages where there is both substitution and frustration, it is expected that a 2D quadrupolar glass will result in analogy to the bulk samples.

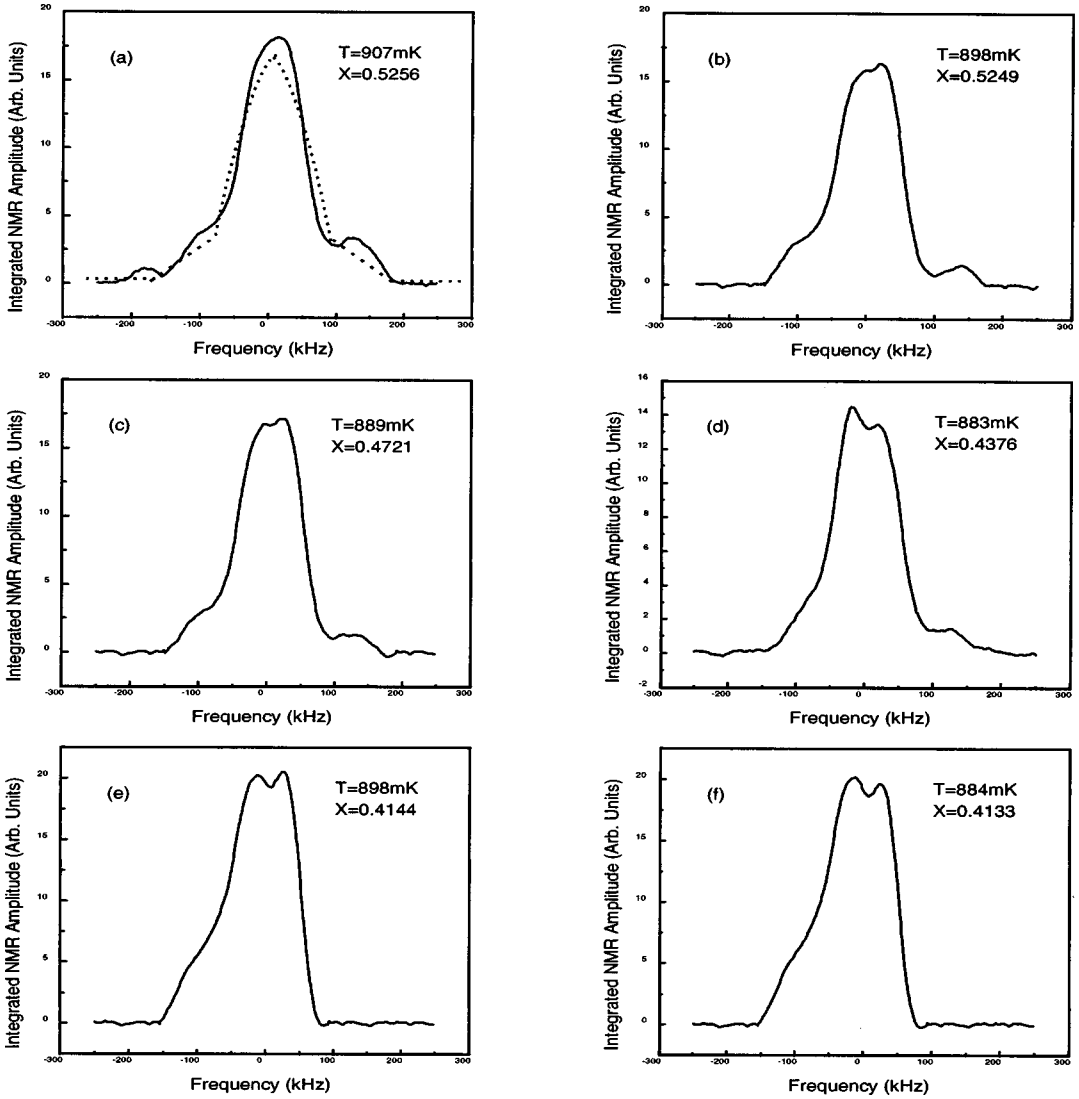

FIG. 16. The evolution of the NMR line shapes for the glass regime for bilayer films of H_2 on BN. The broken line in (a) represents the best fit to the line shape using a quadrupolar glass distribution of order parameters.

Typical NMR absorption spectra for region V of the phase diagram are shown in Fig. 13. These spectra consist of sharp Pake doublet peaks and are best fitted by a long-range periodic ordering, i.e., for $P(\sigma)\simeq\delta(\sigma-\sigma_o)$. For the bilayer films, we interpret the NMR results in terms of a transition to a well-defined orientational ordering for both the first layer and the second layer in the bilayer films. The layers are therefore tightly coupled as far as the orientational degrees of freedom are concerned. This is expected at high X because of the strong anisotropy of the short-range EQQ interactions, and is independent of the translational lattice structure. While herringbone ordering would be expected for monolayers due to the strong interactions with the substrate, we do not expect this type of orientational ordering for bilayers because the strong EQQ interactions between the layers will dominate over the substrate interactions.

The NMR splitting ν_{pp}(T) is given by

$$\nu_{pp}(T)=|D\sigma(3\ \cos^2\beta-1)|, \tag{12}$$

where $\sigma(T)$ is given by Eq. (10), and β is the polar angle specifying the orientation of the magnetic field with respect to the local molecular reference frame. The temperature dependence of the splitting is shown in Fig. 14. We use Eqs. (11)–(13) to determine the effective energy gap Δ and thus the value of V_c for the bilayer films from the best fit to the temperature dependence for ν_{pp}. This fit shown by the dashed line in Fig. 14 yields $|V_c|=1.2\pm0.05$ K. The temperature dependence in Fig. 14 and the mean field predictions are consistent if V_c is negative.

For ortho concentrations $0.4\leqslant X\leqslant 0.57$ and temperatures $0.92<T<1.2$ K, the NMR spectra are distinctly different from those of other regions of the phase diagram. The spectra have two components consisting of a splitting ($\sim$42 kHz) and broad shoulders ($\sim$200 kHz) as shown in Fig. 15. The splitting increases to $\sim$52 kHz, and the amplitude of the shoulders increases by a factor of 2 at $X\simeq 0.39$. These unusual spectra show that there is a mixed phase consisting of a long-range orientational ordering for the second layer (represented by the splitting) and an orientational glass ordering (represented by the shoulders) for the first layer near the substrate. From the growth of the amplitude of the shoulders, we deduce that the orientational ordering for the first layer

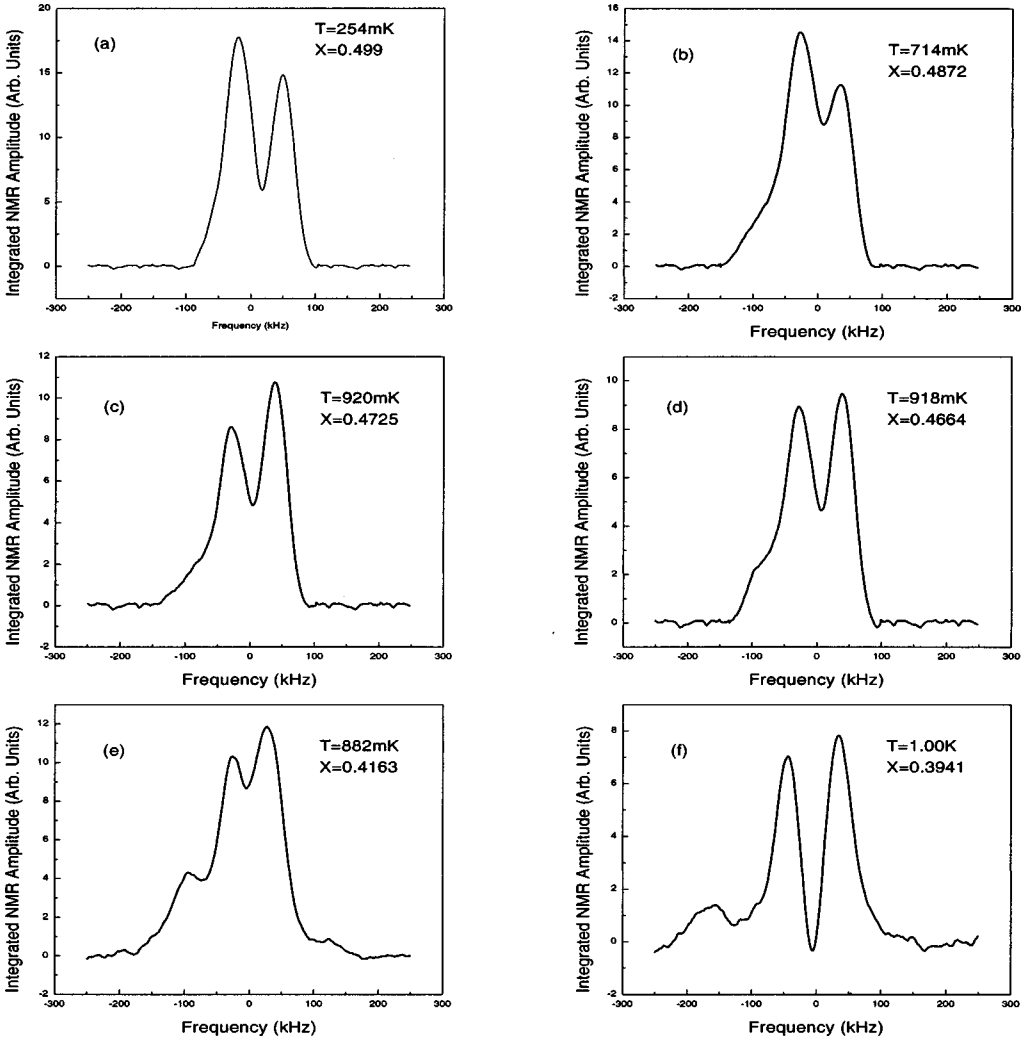

FIG. 17. Typical CW NMR integrated absorption line shapes for bilayers of H_2 on BN for ortho concentration $X<0.55$.

near the substrate increases as X decreases, and at the same time the ordering in the second layer increases, as inferred from the increase in the splitting.

Figure 16 depicts the NMR spectra for an orientational quadrupolar glass ordering. The dashed line in Fig. 16(a) shows a fit to a broad (triangular) distribution of order parameters, $P(\sigma)\propto\sigma$. As the ortho concentration decreases, the central valleys of the spectra fill in slowly and eventually the spectra become similar to the line shapes for the mixed ordered phase. The pure quadrupolar glass ordering regime and the mixed ordering regime disappear for $X\leqslant 0.38$ below which long-range orientational ordering appears.

Figure 17 shows typical NMR absorption line shapes for ortho concentrations $X<0.55$. As X decreases, a doublet spectrum appears below the glass region [Fig. 17(a)], consistent with a long-range orientational ordering (expected from theory to be a pinwheel order). The NMR line shapes show only a single component for long-range ordering and the same ordering occurs for both the first and the second layer. Figure 17(e) has features extending out to ± 200 kHz that resemble the special signatures of the spectra for an orientational herringbone ordering which was observed in the monolayer and submonolayer films of H_2 on BN for low ortho concentrations and low temperatures[70] where the substrate interactions dominate over the EQQ interactions. It is possible that a herringbone ordering could occur in the bilayer films for very low ortho concentrations ($X\sim 0.1$) at very low temperatures ($T<0.1$ K).

A system closely analogous to physisorbed H_2 is physisorbed N_2, which also forms a $\sqrt{3}\times\sqrt{3}$ registered lattice on graphite. N_2 molecules, however, can be treated as classical rotors because of their large moment of inertia. Measurements by Kjems *et al.*[78] of neutron scattering and isotherm experiments of N_2 adsorbed on graphite have been interpreted in terms of structures of the monolayer and of the bilayer that are quite different. They reported that the first layer is characterized as a system with short-range but no long-range order. As the coverage is increased to the second layer there is a transition to ordered planar phases. According to this interpretation, the second layer would induce a drastic change in the first layer: the N_2 molecules of the first layer would be pushed out of their graphite potential wells, either to match another lattice constant or as disordered molecules. However, a different hypothesis has been proposed by Bourdon *et al.*[79] They interpreted the low-temperature phase as an ordered bilayer because the feature of the neutron spectrum produced by the bilayer did not resemble any disordered structure.

For purposes of illustration we show schematic representations of the different orientational orderings deduced from

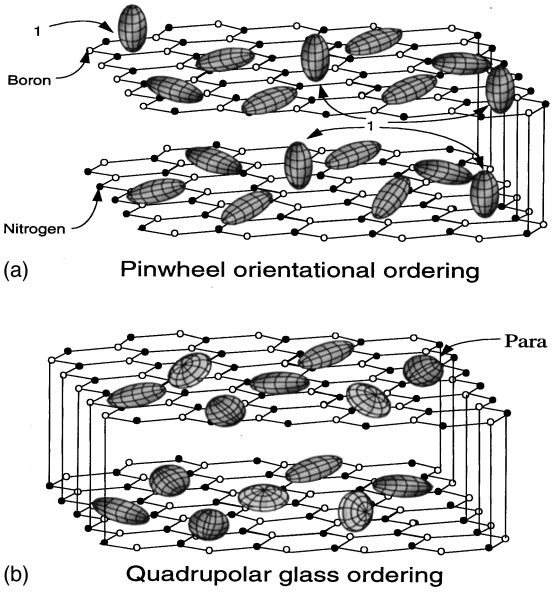

FIG. 18. Schematic representation of different types of ordering of the molecular axes in the bilayer films: (a) pinwheel ordering and (b) quadrupolar glass ordering. The different shapes represent different probabilities for orientations of the molecular axes, and in (a) all are identical (constant σ), while in (b) there is a broad distribution of shapes from prolate ellipsoids ($\sigma \sim 1$) to oblate ellipsoids ($\sigma \sim -\frac{1}{2}$).

the NMR spectra for bilayer films in Figs. 18(a) and 18(b). Figure 18(a) illustrates the long range ordered (inferred pinwheel) phase for both layers that is seen at very low temperatures. Figure 18(b) depicts region III of the phase diagram for the quadrupolar glass ordering observed for both layers at intermediate temperatures.

VI. CONCLUSION

The orientational ordering of ortho-H_2 molecules in a thick film ($\simeq 12$ layers) adsorbed on hexagonal BN is very different from that seen for bulk H_2 and for commensurate monolayers on graphite. We have identified three distinct regimes for the ordering associated with clear changes in the detailed structure of the NMR line shapes: (i) a high-temperature rotationally disordered phase, (ii) an intermediate temperature SCF ordered phase limited to the first 2–3 layers near the substrate, and (iii) at the lowest temperatures a mixed quadrupolar glass state and SCF ordered phase. The analysis of the substrate crystal field ordered spectra shows that the molecules close to the substrate behave as hindered rotors, leading to a large additional width in the spectrum from the spin-orbit coupling ($\vec{I} \cdot \vec{J}$).

The bilayer films exhibit a completely different phase diagram from that observed for the thick films. The predominant features are the existence of a well-defined long-range orientational ordering below $X \sim 0.61$ with a region of coexistence of quadrupolar glass ordering and long-range order for intermediate concentrations and temperatures. The transitions are sharp and the data are best understood if the orientational degrees of freedom of the two layers are tightly coupled together. Unlike the thick films we do not observe a large disordered component that persists to low temperatures. We attribute this to the influence of the substrate crystal fields that induce local orientational ordering in very thin films.

There is a sharp contrast between the orientational ordering observed for both bilayers and 12-layer films and that seen for bulk samples. The enhanced ZPM at the free surface apparently inhibits ordering for relatively thick films while the substrate interactions dominate the behavior for thin films. This behavior is a clear manifestation of the dependence of the ordering in frustrated systems on opposing geometrical constraints due to the presence of the substrate and the free surface. Understanding the different critical concentrations observed to be necessary for long-range orientational ordering and glass ordering for the different geometries is a major challenge for the theory of these frustrated systems.

ACKNOWLEDGMENTS

We gratefully acknowledge the assistance of M. Evans and J. R. Bodart at the beginning of this project. A. D. Migone is thanked for providing information about the preparation of BN, and J. Hamida, E. Genio, and S. Pilla are also thanked for many useful discussions. This work was supported by National Science Foundation Grant Nos. DMR-9216785 and DMR-9623536.

*Present address: Department of Physics, Stanford University, Palo Alto, CA 94305.

[1] Kiho Kim, J. R. Bodart, and N. S. Sullivan, J. Magn. Reson., Ser. A **118**, 28 (1996).
[2] A. B. Harris and A. J. Berlinsky, Can. J. Phys. **57**, 1852 (1979).
[3] P. R. Kubik and W. N. Hardy, Phys. Rev. Lett. **41**, 257 (1978).
[4] N. S. Sullivan, C. M. Edwards, Y. Lin, and D. Zhou, Can. J. Phys. **65**, 1463 (1987).
[5] P. R. Kubik, W. N. Hardy, and H. Glattli, Can. J. Phys. **63**, 605 (1985).
[6] M. D. Evans and N. S. Sullivan, J. Low Temp. Phys. **100**, 551 (1995).
[7] T. Nakamura, Prog. Theoret. Phys. (Kyoto) **14**, 135 (1955).
[8] Isaac F. Silvera, Rev. Mod. Phys. **52**, 393 (1980).
[9] J. Van Kranendonk, *Solid Hydrogen* (Plenum Press, New York, 1983).
[10] J. G. Dash, Contemp. Phys. **30**, 89 (1989).
[11] J. F. van der Veen and J. W. M. Frenken, Surf. Sci. **178**, 382 (1986).
[12] M. Bienfait and J. M. Gay, *Phase Transitions in Surface Films*, edited by J. Taub, G. Torzo, H. J. Lauter, and S. C. Fain (Plenum, New York, 1991), Vol. 2.
[13] P. Zeppenfeld, M. Bienfait, F. C. Liu, O. E. Vilches, and G. Coddens, J. Phys. (France) **51**, 1929 (1990).
[14] M. Maruyama, M. Bienfait, F. C. Liu, Y. M. Liu, O. E. Vilches, and X. Fieutford, Surf. Sci. **283**, 333 (1993).
[15] Jian Ma, Ph.D. dissertation, University of Washington, Seattle, 1989.
[16] Y.M. Liu, Ph.D. dissertation, University of Washington, Seattle, 1993.
[17] J. L. Tell and H. J. Maris, Phys. Rev. B **28**, 5122 (1983).
[18] M. Rall, J. P. Brison, and N. S. Sullivan, Phys. Rev. B **44**, 9639 (1991).

[19] D. F. Brewer, J. Rajendra, N. Sharma, and A. L. Thomson, Physica B **165-166**, 569 (1990).
[20] A. E. Curzon and J. Mascall, Brit. J. Appl. Phys. **16**, 101 (1965).
[21] O. Bostanjoglo and R. Kleinschmidt, J. Chem. Phys. **46**, 2004 (1967).
[22] G. N. Scherhakov, A. I. Prokhvatilov, and I. N. Krupskii, Sov. J. Low Temp. Phys. **11**, 284 (1985).
[23] M. Wagner and D. M. Ceperley, J. Low Temp. Phys. **94**, 161 (1994).
[24] A. Brooks Harris, Phys. Rev. B **1**, 1881 (1970).
[25] M. E. Rose, *Elementary Theory of Angular Momentum* (John Wiley and Sons, New York, 1957).
[26] *Spin-Glasses and Other Frustrated Systems*, edited by D. Chowdury (Princeton University Press, Princeton, NJ, 1986).
[27] K. Binder and J. D. Reger, Adv. Phys. **41**, 547 (1992).
[28] *Statistical Mechanics of Periodic Frustrated Ising Systems*, edited by R. Liebmann (Springer-Verlag, Berlin, 1986).
[29] *Ill Condensed Matter*, edited by R. Balian, R. Maynard, and G. Toulouse (North-Holland, Amsterdam, 1979).
[30] R. O. Poll and G. L. Slazenger, Ann. (N.Y.) Acad. Sci. **279**, 180 (1976).
[31] R. A. H. Austin, K. M. Benson, L. H. Frauenfelder, and I. C. Gunslaus, Biochemistry **41**, 5355 (1975).
[32] H. Sompolinsky, Phys. Rev. Lett. **47**, 935 (1981).
[33] S. R. Shenoy, Physica B **152**, 72 (1988).
[34] *Heidelberg Colloquium on Spin Glasses*, Lecture Notes in Physics Vol. 192 (Springer, Berlin, 1983); *Heidelberg Colloquium on Glassy Dynamics*, edited by J. L. van Hemmen and I. Morgenstern, Lecture Notes in Physics Vol. 275 (Springer, Berlin, 1987).
[35] G. Toulouse, Commun. Phys. **2**, 115 (1977).
[36] K. Binder and A. P. Young, Rev. Mod. Phys. **58**, 801 (1986).
[37] K. Binder, in *Fundamental Problems in Statistical Mechanics V*, edited by E. G. D. Cohen (North-Holland, Amsterdam, 1980), p. 21.
[38] A. P. Ramirez, Annu. Rev. Mater. Sci. **24**, 453 (1994).
[39] M. J. Harris, M. P. Zinkin, Z. Tun, B. M. Wanklyn, and I. P. Swainson, Phys. Rev. Lett. **73**, 189 (1994).
[40] M. Alba, J. Hammann, C. Jacoboni, and C. Pappa, Phys. Lett. **89A**, 423 (1982).
[41] G. Ferey, R. De Pape, M. Leblanc, and J. Pannetier, J. Rev. Chem. Miner. **23**, 474 (1986).
[42] B. P. Cowan and A. J. Kent, Phys. Lett. **106A**, 54 (1984).
[43] The Carborundum Company, Boron Nitride Division, 168 Creekside Drive, Amherst, New York 14228-2027.
[44] Advanced Ceramics Corporation, 11907 Madison Avenue, Lakewood, OH 44107.
[45] Johnson-Matthey, 30 Bond Street, Ward Hill, MA 01835-8099.
[46] F. C. Liu, Y. M. Liu, and O. E. Vilches, Surf. Sci. **294**, 265-272 (1993).
[47] P. Shrestha, M. T. Alkhafaji, M. Lukowitz, G. Yang, and A. D. Migone, Langmuir **10**, 3244 (1994).
[48] M. D. Evans and N. S. Sullivan, J. Low Temp. Phys. **100**, 535 (1995).
[49] T. Crane *et al.*, Physica B **194-196**, 633 (1994).
[50] A. D. Migone, M. T. Alkhafaji, G. Vidali, and M. Karimi, Phys. Rev. B **47**, 6685 (1993).
[51] S. Ross and W. W. Pultz, J. Colloid Sci. **13**, 397 (1958).
[52] R. A. Pierotti, J. Phys. Chem. **66**, 1810 (1962).
[53] R. N. Ramsey and R. A. Pierotti, J. Chem. Phys. **59**, 6163 (1973).
[54] J. Regnier, A. Thomy, and X. Duval, J. Colloid Interface Sci. **70**, 105 (1979).
[55] Y. Grillet and J. Rouquerol, J. Colloid Interface Sci. **77**, 580 (1980).
[56] A. Thomy and X. Duval, Surf. Sci. **90**, 109 (1979).
[57] J. C. Delachaume, M. Coulon, and L. Bonnetain, Surf. Sci. **133**, 365 (1983).
[58] C. Bockel, J. Menaucort, and A. Thomy, J. Phys. (France) **45**, 1391 (1984).
[59] J. P. Lahuerte, J. C. Noiray, M. Obedia, and J. P. Romagan, Surf. Sci. **122**, 330 (1982).
[60] M. T. Alkhafaji and A. D. Migone, Phys. Rev. B **43**, 8741 (1991).
[61] R. A. Wolfson, P. Shrestha, M. T. Alkhafaji, M. M. Lukowitz, G. Yang, and A. D. Migone, Langmuir **12**, 2868 (1996).
[62] Kiho Kim, J. R. Bodart, and N. S. Sullivan, Cryogenics **36**, 311 (1996).
[63] P. Ebey, Y. M. Liu, and O. E. Vilches, Physica B **194-6**, 635 (1994).
[64] MATHEMATICA, Wolfram Research, Champaign, IL 61821.
[65] A. B. Harris and H. Meyer, Can. J. Phys. **63**, 3 (1985).
[66] R. Reif and E. M. Purcell, Physica B **91**, 631 (1953).
[67] A. Dubault and A. P. Legrand, J. Chem. Phys. **61**, 1000 (1974).
[68] A. D. Novaco and J. P. Wroblewski, Phys. Rev. B **39**, 11 364 (1989).
[69] H. Meyer and S. Washburn, J. Low Temp. Phys. **57**, 31 (1984).
[70] Kiho Kim and N. S. Sullivan, Phys. Rev. B **65**, R644 (1997).
[71] D. Clarkson, Xi Qin, and H. Meyer, J. Low Temp. Phys. **91**, 119 (1993).
[72] W. T. Cochran, J. R. Gaines, R. P. McCall, P. E. Sokol, and B. R. Patton, Phys. Rev. Lett. **45**, 1576 (1980).
[73] M. C. Chen and C. P. Slichter, Phys. Rev. B **27**, 278 (1983).
[74] S. F. O'Shea and M. L. Klein, Chem. Phys. Lett. **66**, 381 (1979).
[75] H. Wiechert, in *Excitations in Two-Dimensional and Three-Dimensional Quantum Fluids*, edited by A. G. F. Wyatt and H. J. Lauter (Plenum, New York, 1991), p. 499.
[76] J. Ma, D. L. Kingsbury, F. C. Liu, and O. E. Vilches, Phys. Rev. Lett. **61**, 2348 (1988).
[77] V. Elser, Phys. Rev. Lett. **62**, 2405 (1989).
[78] J. K. Kjems, L. Passell, H. Taub, and J. G. Dash, Phys. Rev. Lett. **32**, 724 (1974).
[79] A. Bourdon, C. Marti, and P. Thorel, Phys. Rev. Lett. **35**, 544 (1975).